RAA 2021 Vol. **21** No. **3**, 73(8pp) doi: 10.1088/1674-4527/21/3/73

http://www.raa-journal.org *http://iopscience.iop.org/raa*

***R**esearch in*
***A**stronomy and*
***A**strophysics*

Possible properties of TeV spectra in PKS 2155–304

Quan-Gui Gao[1,2], Fang-Wu Lu[1,2], Long-Hua Qin[1], Huai-Zhen Li[1], Ju Ma[1], Ji-Yang Ren[1], Hai-Ru Zhao[1] and Ting-Feng Yi[3]

[1] Physics Department, Yuxi Normal University, Yuxi 653100, China; *qlh@yxnu.edu.cn*
[2] Key Laboratory of Astroparticle Physics of Yunnan Province, Kunming 650091, China
[3] Department of Physics, Yunnan Normal University, Kunming 650092, China

Received 2020 April 15; accepted 2020 September 2

Abstract We present a one-zone homogeneous lepton-hadronic model and obtain steady-state spectra by solving the time-dependent equations to study a plausible origin of hard TeV spectra in PKS 2155–304. In this model, we assume a steady electron and proton injection rate in the source and solve the non-linear time-dependent kinematic equations that self-consistently consist of proton-photon interaction, synchrotron radiation of electron/positron pairs and proton, inverse Compton scattering, and synchrotron self-absorption. We employ this model to reproduce the multi-wavelength spectrum of PKS 2155–304, then find that the possible bump located at $E \sim 1$ TeV which may originate from the synchrotron radiation of secondary electrons produced by Bethe-Heitler pair production, resulting in the hard TeV spectrum.

Key words: radiation mechanisms: non-thermal — BL Lacertae objects: individual (PKS 2155–304) — gamma rays: galaxies

1 INTRODUCTION

The high-synchrotron peaked BL Lacertae objects (HBLs) of PKS 2155–304, with the redshift of $z = 0.116$, was discovered in the radio frequencies as part of the Parkes survey (Shimmins & Bolton 1974), and identified as a BL Lac-type source by Hewitt & Burbidge (1980). High-energy (HE) and VHE γ-ray emission of PKS 2155–304 were discovered with EGRET (Vestrand et al. 1995) in the energy range from 30 MeV to 10 GeV, and with the University of Durham Mark 6 telescope above 300 GeV (Chadwick et al. 1999), respectively. During 2008 August 25 and September 6, PKS 2155–304 was observed simultaneously with H.E.S.S., Fermi-LAT, RXTE, and ATOM (Aharonian et al. 2009). Several models have been carried out to interpret this multi-wavelength spectral energy distributions (SEDs) from PKS 2155–304, such as the one-zone synchrotron self-Compton (SSC) model (e.g., Aharonian et al. 2009), the two-zone and stratified jet SSC model (e.g., Abramowski et al. 2012), and the proton synchrotron model (e.g., Petropoulou 2014).

An interesting feature in the observation of SEDs of PKS 2155–304 is that there is a possible bump located at $E \sim 1$ TeV, named as "cascade bump" by Zech et al. (2017). The study offered by Zech et al. (2017) shows that the cascade bump of PKS 2155–304 will appear when the value of $\eta = u_p/u_B$ is sufficiently high, where u_p and u_B are the energy densities of the proton and magnified in the jet, respectively. In this case, compared with the proton synchrotron emission, the proton - photon interactions are indeed important, the muon synchrotron component becomes prominent and the "cascade bump" feature appears.

Bethe-Heitler pair production is often neglected in astrophysics since it is not associated with neutrino and neutron production, and thus, the weight of Bethe-Heitler pair production involved in blazar emission models was overlooked (e.g., Böttcher et al. 2013; Weidinger & Spanier 2015; Diltz & Böttcher 2015). However, the physical process of proton - photon pion production attracted more attention (e.g., Sikora et al. 1987; Kirk & Mastichiadis 1989; Begelman et al. 1990; Waxman & Bahcall 1997; Atoyan & Dermer 2001, 2003). Recently, several articles have been carried out to study the blazar spectrum using Bethe-Heitler pair production (e.g., Mastichiadis et al. 2005; Petropoulou & Mastichiadis 2015; Cerruti et al. 2015; Yan & Zhang 2015; Zheng et al. 2016; Zech et al. 2017). In this paper, we focus on the contribution of pairs produced by the Bethe-Heitler pair production process to the SED of PKS 2155–304.

In the next section, we briefly review the model, then give our numerical results of the model in Section 3, and employ the model to study PKS 2155–304 in Section 4, finally we give our conclusion and discussion in Section 5. Throughout the paper, a flat cosmology with $H_0 = 70\ \mathrm{km\ s^{-1}\ Mpc^{-1}}$, $\Omega_\mathrm{m} = 0.3$, and $\Omega_\Lambda = 0.7$ is assumed. The luminosity distance to the source is 539.6 Mpc at $z = 0.116$. The model of Franceschini et al. (2008) is used for the extragalactic background light (EBL) absorption.

2 THE MODEL

We consider a spherical blob with a radius R, where the magnetic field strength and a Doppler factor are B and δ, respectively. We then let L^e_inj and L^p_inj be the luminosity of relativistic electrons and protons injected into the source. The relationship between the injected luminosity (L^i_inj) and injection compactness (ℓ^i_inj) can be expressed as (e.g., Petropoulou & Mastichiadis 2011; Mastichiadis et al. 2013)

$$\ell^i_\mathrm{inj} = \frac{\sigma_\mathrm{T} L^i_\mathrm{inj}}{4\pi R m_i c^3}\ , \tag{1}$$

where $i = \mathrm{e, p}$; σ_T and c are the Thomson cross-section and light speed, respectively. Also, we use the methods offered by Diltz & Böttcher (2015) and Mastichiadis & Kirk (1995) to calculate the synchrotron radiation of protons and electrons, as well as the rest of the physical processes. Based on the electrons lose their energies through the synchrotron self-Compton mechanism. Furthermore, the electrons and protons will lose their energies through physical and radiation process such as SSC mechanism and proton-photon interaction, and we use the well-known evolution equations (e.g., Mastichiadis & Kirk 1995; Dimitrakoudis et al. 2012; Weidinger & Spanier 2015; Diltz & Böttcher 2015) of protons, electrons, and photons in a comoving frame as

$$\frac{\partial n_\mathrm{p}(\gamma_\mathrm{p},t)}{\partial t} + \frac{n_\mathrm{p}}{t_\mathrm{p,esc}} = L^\mathrm{p}_{\mathrm{p}\gamma\to\mathrm{pee}} + L^\mathrm{p}_{\mathrm{p}\gamma\to\mathrm{p}\pi} + L^\mathrm{p}_\mathrm{p,syn} + Q^\mathrm{p}_\mathrm{inj}, \tag{2}$$

$$\frac{\partial n_\mathrm{e}(\gamma_\mathrm{e},t)}{\partial t} + \frac{n_\mathrm{e}}{t_\mathrm{e,esc}} = L^\mathrm{e}_\mathrm{e,syn} + L^\mathrm{e}_\mathrm{ics} + Q^\mathrm{e}_{\mathrm{p}\gamma\to\mathrm{pee}} + Q^\mathrm{e}_{\mathrm{p}\gamma\to\mathrm{p}\pi} + Q^\mathrm{e}_\mathrm{inj}, \tag{3}$$

and

$$\frac{\partial n_\gamma(x,t)}{\partial t} + \frac{n_\gamma}{t_{\gamma,\mathrm{esc}}} = Q^\gamma_\mathrm{p,syn} + Q^\gamma_\mathrm{e,syn} + Q^\gamma_\mathrm{ics} + L^\gamma_\mathrm{ssa} + Q^\gamma_{\mathrm{p}\gamma\to\mathrm{p}\pi}. \tag{4}$$

Here n_p, n_e and n_γ are the differential number densities of proton, electron and photon in units of a volume element of size $\sigma_\mathrm{T} R$, γ_p and γ_e represent the Lorentz factor of proton and electron, respectively, $x = h\nu/(m_e c^2)$ is the dimensionless photon frequency. The escape timescales of protons, electrons and photons are $t_\mathrm{p,esc}$, $t_\mathrm{e,esc}$ and $t_{\gamma,\mathrm{esc}}$ and can be roughly taken as the crossing time $t_\mathrm{cross} = R/c$. Furthermore, there are six physical processes in the right sides of Equations (2), (3) and (4) have been taken into account:

(1) Proton synchrotron emission which represents a loss term for protons $L^\mathrm{p}_\mathrm{p,syn}$ and an injection term for photons $Q^\gamma_\mathrm{p,syn}$.

(2) Electron synchrotron emission which represents a loss term for electrons $L^\mathrm{e}_\mathrm{e,syn}$ and a source term for photons $Q^\gamma_\mathrm{e,syn}$.

(3) Bethe-Heitler pair production which represents an energy loss term for protons $L^\mathrm{p}_{\mathrm{p}\gamma\to\mathrm{pee}}$ and an injection term for electrons $Q^\mathrm{e}_{\mathrm{p}\gamma\to\mathrm{pee}}$.

(4) Proton-proton pion production which represents a loss term for protons $L^\mathrm{p}_{\mathrm{p}\gamma\to\mathrm{p}\pi}$ and source terms for electrons $Q^\mathrm{e}_{\mathrm{p}\gamma\to\mathrm{p}\pi}$ and photons $Q^\gamma_{\mathrm{p}\gamma\to\mathrm{p}\pi}$.

(5) Inverse Compton scattering (in both the Thomson and Klein-Nishina regimes) which represents a loss term for electrons $L^\mathrm{e}_\mathrm{ics}$ and a source term for photons Q^γ_ics.

(6) Synchrotron self-absorption which represents a loss term for photons L^γ_ssa. $Q^\mathrm{e}_\mathrm{inj}$ and $Q^\mathrm{p}_\mathrm{inj}$ are the injection terms of electrons and protons, respectively. Here, we assume that the relativistic electrons and protons have a power-law distribution, the complete forms are the same as equations (3) and (5) in Gao et al. (2017). For more details about this special calculation progress, we recommend to refer Diltz & Böttcher (2015) and Mastichiadis & Kirk (1995). However, only the method of BH pair production process is described here.

A proton of dimensionless energy γ_p interacts with a photon with energy $x = h\nu/m_\mathrm{e}c^2$ in a Coulomb field if the threshold condition $\gamma_\mathrm{p} x \geq 2$ is satisfied, then the $\mathrm{e}^\pm$ will be produced. The fractional energy loss of proton can be written as

$$L^\mathrm{p}_{\mathrm{p}\gamma\to\mathrm{pee}} = \frac{2m_\mathrm{e}}{m_\mathrm{p}}\frac{\partial}{\partial\gamma}[\gamma_\mathrm{p} n_\mathrm{p}(\gamma_\mathrm{p},t) \times \int_{2/\gamma_\mathrm{p}}^{\infty} n_\gamma(x,t)\sigma_\mathrm{pe}(x\gamma_\mathrm{p})dx], \tag{5}$$

where $\sigma_\mathrm{pe}(x')$ is the Bethe-Heitler cross-section in units of σ_T as a function of the photon energy x' in proton rest frame. To calculate the cross-section of $\sigma_\mathrm{pe}(x')$, we use the analytical approximations of the equations A1 and A2 in appendix A given by Begelman et al. (1990). But it needs a slightly modification in our calculation, for lower photon

energies

$$\sigma_{\rm pe}(x') = \frac{1}{\sigma_T} 1.2135 \times 10^{-27} (\frac{x'-2}{2})^3 \times (1 + \frac{1}{2}\eta + \frac{23}{40}\eta^2 + \frac{37}{120}\eta^3 + \frac{61}{192}\eta^4 + \cdots) \quad (6)$$

with $\eta = (x'-2)/(x'+2)$, and for higher energies,

$$\begin{aligned}\sigma_{\rm pe}(x') =& \frac{1}{\sigma_T} 5.7938 \times 10^{-28} [3.1111 \ln 2x' - 8.0741 \\ &+ (\frac{2}{x'})^2 (2.7101 \ln 2x' - \ln^2 2x' \\ &+ 0.6667 \ln^3 2x' + 0.5490) \\ &- (\frac{2}{x'})^4 (0.1875 \ln 2x' + 0.1250) \\ &- (\frac{2}{x'})^6 (0.0126 \ln 2x' - 0.0056) + \cdots],\end{aligned} \quad (7)$$

as given by Begelman et al. (1990). Noted that this method will contain the fractional error between 1.1×10^{-3} and 4.4×10^{-5} at $x' \sim 4$. The injection term for electrons $Q^{\rm e}_{\rm p\gamma\to pee}$ of BH pair production can be written as

$$Q^{\rm e}_{\rm p\gamma\to pee}(\gamma_{\rm e}, t) = 2 n_{\rm p}(\gamma_{\rm p}, t) \times \int_{2/\gamma_{\rm p}}^{\infty} n_\gamma(x, t) \sigma_{\rm pe}(x\gamma_{\rm p}) dx. \quad (8)$$

It should be pointed out that the electrons and positrons are not distinguished here.

3 SPECTRAL SIGNATURES

Once the electrons and protons injected into a spherical blob with a radius of R, and a tangled magnetic field strength B, the electrons will lose their energies through synchrotron, IC processes. The protons lose their energies through synchrotron radiation, proton - photon pair production (i.e., Bethe-Heitler pair production), and proton - photon pion production; the process of BH pair production will produce $\rm e^{\pm}$ as an injection term in electron equation, Equation (3), which will take place synchrotron and IC radiation combined with the primary electrons. For proton - photon pion production, the method offered by Mastichiadis & Kirk (1995) and basic channels are considered:

(1) $p + \gamma \to p + \pi^0$,
(2) $p + \gamma \to p + \pi^+$.

These two channels will lose energies as a sink term in the proton equation (Eq. (2)). The neutral pion (π^0) originated from the channels (1) decay essentially instantaneously into γ-rays and will provide a source term in the photon equation (Eq. (4)). Three neutrinos and a positron are created in the decay chain of a π^+ from the channel (2), assuming again that these are produced with equal energies, then a source term of the position in Equation (3) can be obtained. In this paper, the radiation of neutrinos has not been taken into account.

Table 1 Parameter Values of Fig. 1

Parameter	Symbol	Value
Electron injection compactness	$\ell^{\rm e}_{\rm inj}$	3×10^{-4}
Electron injection minimum energy	$\gamma_{\rm e,min}$	1.2×10^3
Electron injection maximum energy	$\gamma_{\rm e,max}$	4×10^4
Electron injection spectral index	p	2.4
Proton injection compactness	$\ell^{\rm p}_{\rm inj}$	1.6×10^{-6}
Proton injection minimum energy	$\gamma_{\rm p,min}$	1×10^6
Proton injection maximum energy	$\gamma_{\rm p,max}$	7×10^9
Proton injection spectral index	q	2.4
Magnetic field	B	70 G
Radius of emission region	R	9.5×10^{15} cm

Equations (2), (3) and (4) can be sloved self-consistently, and the radiation spectra of photon are shown in Figure 1. The left panel shows the different components of photon SEDs in a steady-state. The black solid curve represents the total spectrum of the photon, the red and blue curves are the corresponding synchrotron of electrons/positrons (include primary electrons and secondary pairs) and protons respectively, the green line indicates the IC spectrum of electrons/positrons (the same electron population of synchrotron), the orange curve represents the photon spectrum from proton - photon pion production, the right panel shows the comparison of photon spectra include Bethe-Heitler pair production with which without Bethe-Heitler pair production, the solid line represents the photon spectrum include the Bethe-Heitler pair production, the dashed line is corresponding the photon spectrum without Bethe-Heitler pair production. The results indicate that the synchrotron of electrons/positrons which form Bethe-Heitler pair production will influence the photon spectrum in the energy range of $x \sim 10^{-3}$ to $x \sim 10^8$ and dominate the radiation at $3 \times 10^5 \lesssim x \lesssim 10^7$. Note that a "bump" appeared around the energy range of $x \sim 10^6$.

The steady-state spectra are due to the competition of all physical processes by self-consistent solving the Equations (2), (3) and (4). Based on the chosen set of parameters (see Table 1), the contribution of inverse Compton scattering is nonsignificant in the model (see the left panel of Fig. 1). One can find that, comparing to the total spectra with the inverse Compton spectra, the latter is an order of magnitude lower at least. Moreover, the proton-photon pion production mainly influences the energy range of $x > 10^7$ which will be almost entirely absorbed by EBL. Particularly, for the proton-photon interaction, Bethe-Heitler pair production, and proton-photon pion production are responsible for the range of radiation spectra $10^5 \lesssim x \lesssim 10^8$ and $10^8 \lesssim x \lesssim 10^{12}$, respectively,

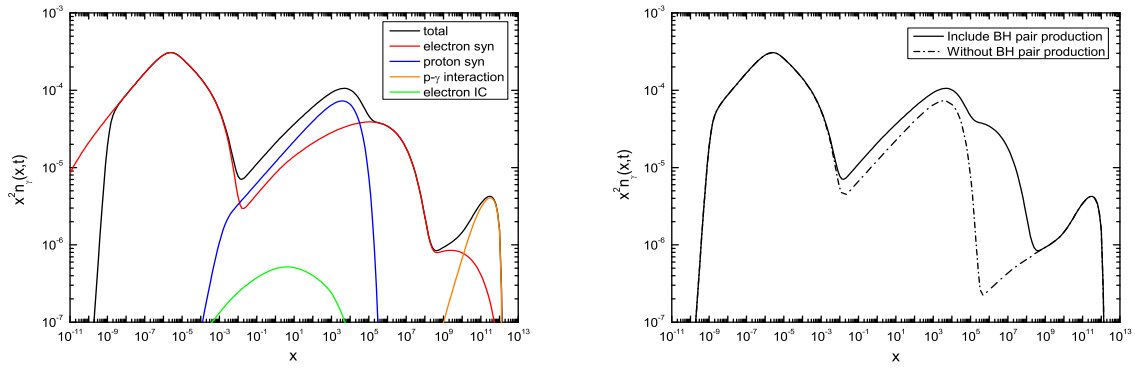

Fig. 1 *Left panel*: Different components of photon SED in steady state. *Right panel*: The comparison of photon SED include Bethe-Heitler pair production (*solid line*) with which without Bethe-Heitler pair production (*dashed line*). The model parameters are listed in Table 1.

due to the competition. Furthermore, a steep spectrum of protons is adopted that lead to most proton energy is contained in the regime below the photo-pion production threshold, then the relative suppression of photo-pion production to Bethe-Heitler process makes the luminosity due to pion production at least one order magnitude smaller than that due to the Bethe-Heitler process. It should be pointed out that, to save the computational cost, the approximate expressions are adopted for inverse Compton scattering and proton-photon pion production in this paper; for detailed methods of these processes please refer to Mastichiadis & Kirk (1995).

In Figure 2, the influence of parameters change on spectra are shown. We can find that the "bump" around $x \sim 10^6$ will not appear if $B \backsimeq 10$ G, and will appear from 30 G to 110 G. If $B > 110$ G, with the increasing of the magnetic field, the "bump" becomes unclear. Therefore, dozens of Gauss of the magnetic field are chosen in this model (Some authors adopted the magnetic field as high as 150 G (e.g., Diltz & Böttcher 2015) in blazar model, so the value of he magnetic field seems reasonable). It is interesting that the synchrotron radiation by Bethe-Heitler pairs decreases when the magnetic strength increases, this is because of higher magnetic strength causing greater energy loss through synchrotron emission of protons. Thus, the energy of pairs which produced by Bethe-Heitler pair production will decrease with the magnetic strength increase, resulting in the synchrotron radiation by Bethe-Heitler pairs decreases (see the upper left panel of Fig. 2). Because of the contribution due to the synchrotron emission of secondary electrons that from Bethe-Heitler pair production with the increasing proton injection spectral index become more and more obvious, the changes of proton injection spectral index mainly lead to the changes of the spectral index in the GeV band of photons. The changes in proton injection maximum energy and proton injection compactness only lead to the changes in photon flux. However, the shape of the spectra will not be changed. The increasing of proton injection maximum energy will lead to the increasing of the flux in the γ-ray band. The increasing of proton injection compactness will lead to the increasing of the flux from X-ray to γ-ray bands. All the parameters in Figure 2 are consistent with those in Table 1, except for the parameters marked on the figure.

According to the influence of parameters change on spectra, using the following methods select the model parameters in the practical applications.

- The magnetic field of the emission region is fixed as dozens of Gauss.
- Take advantage of the observations of GeV band constrains the spectral index of protons. We suppose that the electrons and protons are co-accelerated— the spectral index of electrons (p) is same as the spectrum index of protons (q) before cooling.
- After the Doppler factor is determined, according to observed TeV spectra adjust the maximum energy of injected protons.
- Adjust the injected compactness of protons based on the observed spectra of γ-rays.
- Except the spectral index, the other parameters of electrons are adjusted on the basis of the observed data of optical to X-ray bands.
- The minimum energy of injected protons does not have an obvious effect on the energy spectra. However, we need to make sure that the total luminosity cannot exceed the Eddington luminosity.

4 APPLICATION TO PKS 2155–304

We use the method described by Section 2 to interpret the broadband SEDs of PKS 2155–304 as well as its possible "cascade bump". Furthermore, we transform the SEDs from the comoving frame to the observer's frame

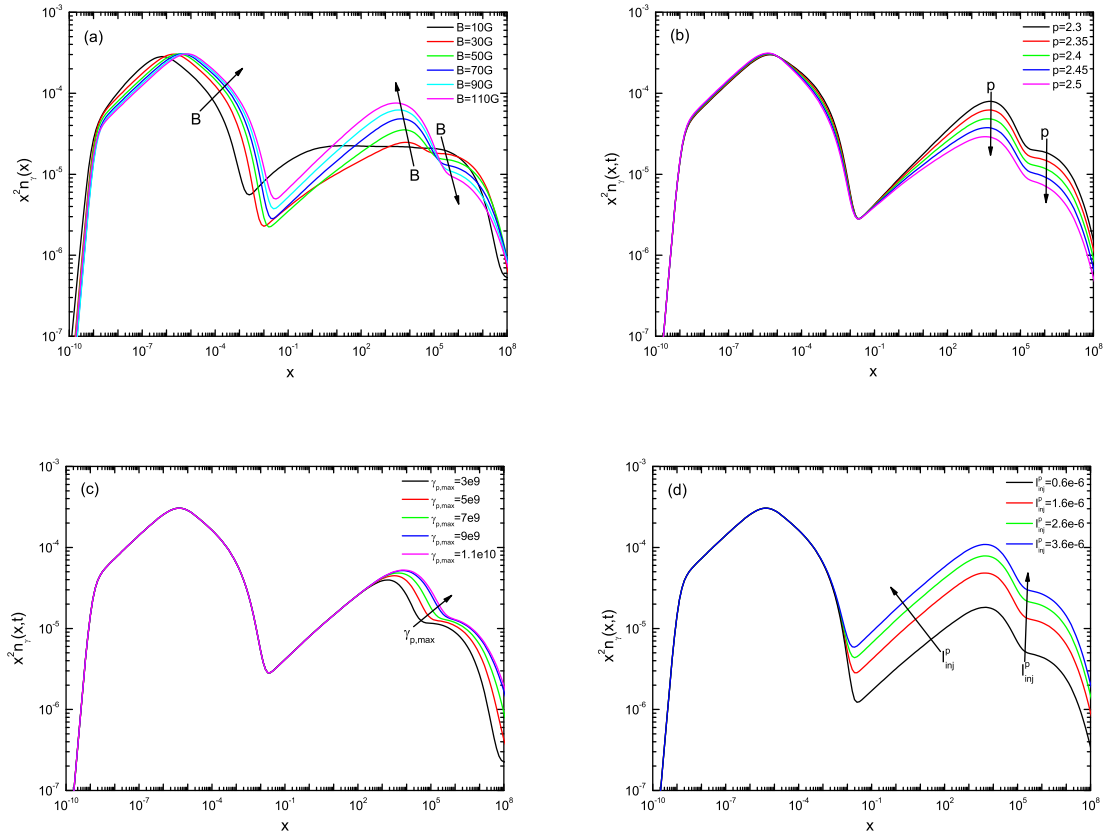

Fig. 2 The influence of parameters change on spectra. From (a) to (d), the spectra change with the parameters of magnetic field, spectral index, proton injection maximum energy, proton injection compactness changes are shown.

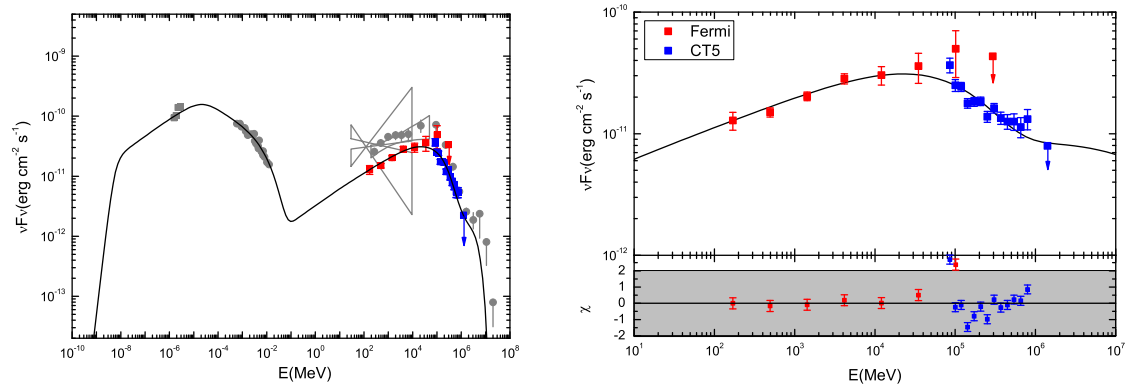

Fig. 3 *Left panel*: Comparison of model results with the observed SEDs of PKS 2155–304. *Right panel*: Intrinsic spectra of PKS 2155–304. The black line is corresponding to the model results, the 95% confidence region is shown by the shaded area in the bottom.

(Diltz & Böttcher 2014). In Figure 3, the blue squares are obtained from the H.E.S.S. II mono analysis (MJD 56403 - 56601) and the red squares represent the contemporaneous Fermi-LAT measurements (all these observational data are from H.E.S.S. Collaboration et al. 2017[1]). The grey data points (MJD 54704 – 54715) are extracted from Aharonian et al. (2009). The fitting results of PKS 2155–304 are shown in the left and right panel of Figure 3. The left panel shows the multiwavelength results, the right panel corresponding to the intrinsic spectra of γ-rays, and the residuals are shown in the bottom. Except for the Doppler factor being set as $\delta = 11$, the other

[1] https://www.mpi-hd.mpg.de/hfm/HESS/pages/publications/auxiliary/PKS2155_HESSII_auxinfo

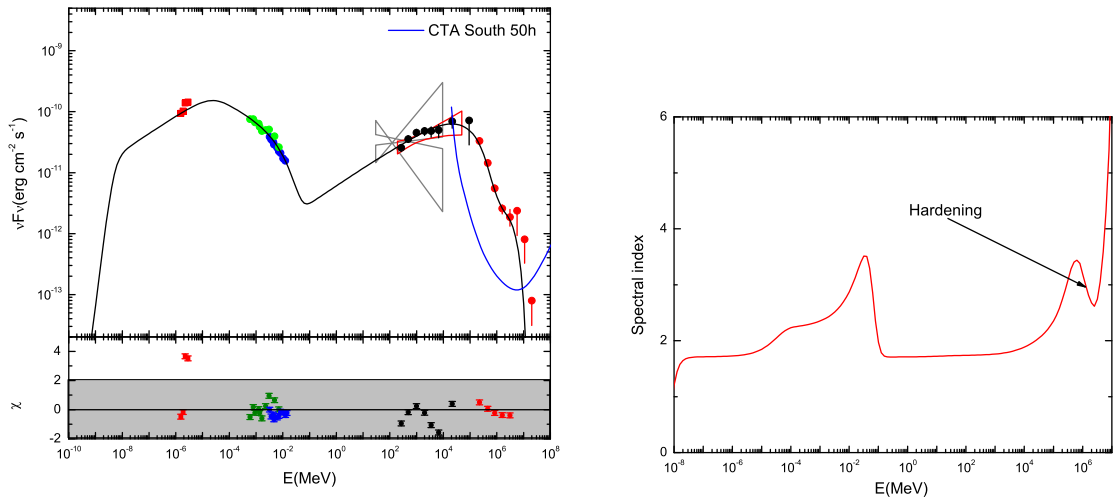

Fig. 4 *Left panel*: Comparison of model results with the simultaneous observed SEDs of PKS 2155–304. All points are extracted from Aharonian et al. (2009). Except $\ell_{\rm inj}^{p} = 3 \times 10^{-6}$, $B = 75$ G and $R = 1 \times 10^{16}$ cm, the other parameters are the same as Fig. 3. *Right panel*: The spectral index of model.

parameters are the same as Table 1. In this case, the power carried along the jet in the form of a magnetic field (i.e., the Poynting flux) is $L_B = 6.626 \times 10^{45}$ erg s^{-1}, the injection luminosity of protons is $L_{\rm inj}^{\rm p} = 1.291 \times 10^{43}$ egs s^{-1} and the injection luminosity of electrons is $L_{\rm inj}^{\rm e} = 1.323 \times 10^{42}$ erg s^{-1}, the corresponding energy densities are $u_B \approx 195$ erg cm^{-3}, $u_{\rm p} \approx 0.4$ erg cm^{-3} and $u_{\rm e} \approx 0.04$ erg cm^{-3} the lower cutoff of the proton Lorentz factor uses an ad-hoc value as $\gamma_{\rm p,min} = 1 \times 10^6$. This value can be adjusted from $\gamma_{\rm p,min} = 1$ to $\gamma_{\rm p,min} = 1 \times 10^6$ that will not make the jet power exceed the Eddington luminosity, the influence with the change of $\gamma_{\rm p,min}$ has been fully discussed in our previous article, and for details please refer to Gao et al. (2018).

As a comparison, the simultaneous observed data are fitted by the model calculation (solid line), the results are shown in the left panel of Figure 4 and the residuals are shown in the bottom. All the observational data are extracted from Aharonian et al. (2009). From low to high energies: optical measurements (red filled squares) from ATOM, combined RXTE and Swift X-ray measurements (green & blue filled circles), and gamma-ray observations (black filled circles) by Fermi-LAT and H.E.S.S. (red filled circles) in the GeV and TeV energy bands, respectively. The red butterfly is the actual Fermi spectrum for the period MJD 54704–54715 and the grey ones show EGRET measurements. To reproduce the simultaneous observed SED, three principles are followed to adjust the parameters based on Table 1:

– The criterion to adjust the parameters of electrons by the basic observed data of optical to X-ray bands are the primary electrons, which only influence the SED of optical to X-ray bands;
– Try to avoid to adjust the parameters of protons except for injection compactness, which stands for the change of flux from GeV to TeV bands, originating from the change of proton compactness;
– Keep the indices of electrons consistent with protons, which represents that electrons and protons are co-accelerated.

We find that the simultaneous observed data can be reproduced well with a slight adjustment of the parameters based on Table 1, and the corresponding parameters listed in Table 2. In this case, the power carried along the jet in the form of a magnetic field (i.e. the Poynting flux) is $L_B = 8.007 \times 10^{45}$ erg s^{-1}, the injection luminosity of protons is $L_{\rm inj}^{\rm p} = 2.548 \times 10^{43}$ erg s^{-1} and the injection luminosity of electrons is $L_{\rm inj}^{\rm e} = 1.067 \times 10^{42}$ erg s^{-1}, the corresponding energy densities are $u_B \approx 224$ erg cm^{-3}, $u_{\rm p} \approx 0.7$ erg cm^{-3} and $u_{\rm e} \approx 0.03$ erg cm^{-3}, respectively. The results indicate that the optical and X-ray bands are from the synchrotron radiation of primary and secondary electrons. In the energy range of 0.1 MeV to $\sim 2 \times 10^7$ MeV, the radiation is produced by the synchrotron radiation of primary protons and secondary electrons. In particular, the bump located at $E \sim 1$ TeV is contributed by the synchrotron radiation of secondary electrons originated from Bethe-Heitler pair production. Due to the high resolution of the Cherenkov Telescope Array (CTA)[2], this energy spectrum property

[2] This research has made use of the CTA instrument response functions provided by the CTA Consortium and Observatory,

Table 2 Parameter Values of Fig. 4

Parameter	Symbol	Value
Electron injection compactness	$\ell_{\rm inj}^{\rm e}$	2.3×10^{-4}
Electron injection minimum energy	$\gamma_{\rm e,min}$	1.2×10^{3}
Electron injection maximum energy	$\gamma_{\rm e,max}$	3.8×10^{4}
Electron injection spectral index	p	2.4
Proton injection compactness	$\ell_{\rm inj}^{\rm p}$	3×10^{-6}
Proton injection minimum energy	$\gamma_{\rm p,min}$	1×10^{6}
Proton injection maximum energy	$\gamma_{\rm p,max}$	7×10^{9}
Proton injection spectral index	q	2.4
Magnetic field	B	75 G
Radius of emission region	R	1×10^{16} cm
Doppler factor	δ	11

can be observed by it in the future. For comparison, the 50 h differential sensitivity goal of CTA is shown. The residuals are shown in the bottom of the left panel of Figure 4, the grey area corresponding to $-2 < \chi < 2$, which stands for the 95% confidence region. Furthermore, comparing the observations of Aharonian et al. (2009) with H.E.S.S. Collaboration et al. (2017), we find that the major differences are the flux in the energy range of 0.1 – 300 GeV, which indicates that the flux change of orphan GeV band only results from the changes of a few parameters, namely the injection compactness of proton ($\ell_{\rm inj}^{p}$), magnetic field (B) and radius (R) of emission region in this work. Our results imply that the variability of the GeV band can be reproduced by the change of injection compactness of proton and emission region parameters.

The spectral index of the model is shown in the right panel of Figure 4 and one can find that in the $\sim 0.6 - 2$ TeV energy range, the spectral index of photon decrease rapidly and leads to TeV spectrum hardening. It should be pointed out that only when the magnetic field strength is relatively large (say dozens of Gauss), the synchrotron emission of secondary electrons from Bethe-Heitler pair production is dominated in the TeV energy range and leads to TeV spectrum hardening. This is because the synchrotron emission of relativistic protons is mainly responsible for the $0.1 - 5 \times 10^4$ Mev energy range, and the proton-photon pion production is responsible for the energy range of $E \gtrsim 10^7$ MeV, between 5×10^4 MeV and 10^7 MeV, and the radiation is dominated by the synchrotron emission of secondary electrons which is produced by Bethe-Heitler pair production.

5 SUMMARY AND DISCUSSION

In this paper, we have introduced a self-consistent Lepto-Hadronic emission model in the blazar jets and obtained steady-state spectra by solving the time-dependent equations. Taking all relevant processes into account, namely synchrotron emission of electrons and protons, synchrotron self-absorption, inverse Compton scattering, Bethe-Heitler pair production, and proton-photon pion production. In this model, the primary protons produce the γ-ray through the synchrotron radiation, the synchrotron radiation of primary electron results in the soft photons, meanwhile, the relativistic protons lose their energies through proton-photon interaction which include Bethe-Heitler pair production and proton - photon pion production. The secondary electrons produced by Bethe-Heitler pair production mainly influence the spectra of the photon with the energy of $x \sim 10^{-3}$ to 10^8 through synchrotron radiation (see the right panel of Fig. 1). In particular, the flux of synchrotron emission of protons begin to decrease obviously at $x = 10^4$, but the flux of synchrotron emission of secondary electrons begin to decrease obviously until $x \gtrsim 10^6$. One can find that a "bump" will appear if x is around 1×10^6.

Our model has been applied to investigate the SED of the VHE blazar PKS 2155–304. For a power-law electron and proton injection form, our results show that the primary electron mainly influences the SED from radio to X-ray bands, while high energy γ-ray SED is mainly determined by the synchrotron radiation protons and secondary pairs which from Bethe-Heitler pair production. However, the proton - photon pion production will influence the higher energy range of the SED ($E \gtrsim 10^7$ MeV). Particularly, the bump at $E \sim 1$ TeV can be explained by the synchrotron radiation of secondary pairs produced by Bethe-Heitler pair production. This property of spectra appears only when the maximum of proton energy is relatively high ($\gamma_{\rm p} \sim 7 \times 10^9$) and the magnetic field strength is relatively large ($B \sim 70$ G). In the case of the maximum of proton energy relatively small (say $\gamma_p \sim 10^7$), the spectrum of the synchrotron emission of $e^{\pm}$ will fill the gap between the X-rays and γ-rays (Petropoulou & Mastichiadis 2015), and the TeV spectrum are dominated by the proton-photon pion production. If the energy of proton exceeds $\gamma_{\rm p} > 10^{10}$ and the magnetic field strength is large enough, the TeV spectrum will be covered by the synchrotron emission of relativistic protons in our model. However, the feature of TeV spectrum hardening will appear when the parameters (for example, $\gamma_p \sim 7 \times 10^9$, $B \sim 70$ G, and $\delta \sim 10$) are appropriate. The "bump" will be detected by CTA in the future. But the "bump" may also originate from the other processes such as μ synchrotron or $\pi^{\pm}$ cascade (Cerruti et al. 2015; Zech et al. 2017), the origin of radiation can be distinguished associated with the neutrino observations since the μ and $\pi^{\pm}$ are produced in the process of proton-photon pion production, such

see *http://www.cta-observatory.org/science/cta-performance/* (version prod3b-v2) for more details.

as the possible association with the high-energy neutrino event IceCube-170922A has sparked interest in the blazar TXS 0506+056 (e.g., Aartsen et al. 2018; Britzen et al. 2019; Kovalev et al. 2020). In contrast, Bethe-Heitler pair production does not produce neutrinos. we suggest that if the accompanying neutrino radiation of PKS 2155–304 cannot be observed, our model is the reliable explanation of the emission from PKS 2155–304. Moreover, the hardened feature of the spectrum will disappear under certain conditions, e.g., larger luminosity distance, which will lead to the "cascade bump" feature disappearing because of EBL absorption.

As can be seen in Figure 4, synchrotron emission by secondary electrons can produce a spectral hardening in the observed TeV spectrum. The absorption of γ-ray photons is neglected in this research. Indeed, the γ-γ annihilation will absorb a fraction of γ-ray photons. However, it does not make the "bump" disappear. Moreover, the Eddington luminosity of PKS 2155–304 is $L_{\rm edd\ pks\ 2155-304} \approx 2 \times 10^{46}$ erg s^{-1}, which is corresponding to $M_{\rm BH\ pks\ 2155-304} \approx 2 \times 10^{8} M_{\odot}$ (e.g., McLure & Dunlop 2002; Rieger & Volpe 2010). Note that the jet power will be no more than 8.1×10^{45} erg s^{-1}, which means that the parameters are reasonable.

Acknowledgements We thank the anonymous referee for his/her very constructive suggestions. This work is partially supported by the National Natural Science Foundation of China (Grant Nos. 12063006, 11803027 and 11863007), Yunnan Local Colleges Applied Basic Research Projects (Grant Nos. 202001BA070001-031, 2017FH001-102, 2018FH001-015, 2019FH001-012 and 2019FH001-076), and Science Research Foundation of Yunnan Education Department of China (Grant Nos. 2017ZZX177, 2018JS422 and 2019J0733). The author (QLH) gratefully acknowledges the financial support from the Hundred Talents Program of Yuxi (Grant Nos. 2019).

References

Aartsen, M. G., Ackermann, M., et al. 2018, Science, 361, eaat1378
Abramowski, A., Acero, F., Aharonian, F., et al. 2012, A&A, 539, A149
Aharonian, F., et al. 2009, ApJ, 696, 150
Atoyan A., & Dermer C. D. 2001, Phys. Rev. Lett., 87, 221102
Atoyan A. M., & Dermer C. D. 2003, ApJ, 586, 79
Begelman M. C., Rudak B., & Sikora M. 1990, ApJ, 362, 38
Böttcher, M., Reimer, A., Sweeney, K., & Prakash, A. 2013, ApJ, 768, 54
Britzen S., Fendt C., Böttcher, M., et al. 2019, A&A, 630, A103
Cerruti, M., Zech, A., Boisson, C., & Inoue, S. 2015, MNRAS, 448, 910
Chadwick, P. M., Lyons, K., McComb, T. J. L., et al. 1999, ApJ, 513, 161
Diltz, C., & Böttcher, M. 2014, JHEAp, 1, 63
Diltz, C., & Böttcher, M. 2015, ApJ, 802, 133
Dimitrakoudis S., Mastichiadis A., Protheroe R. J., & Reimer A. 2012, A & A, 546, A120
Gao, Q. G., Lu, F. W., & Zhang, L. 2017, MNRAS, 464, 1704
Gao, Q. G., Lu, F. W., Ma, J., et al. 2018, Ap&ss, 363, 119
H.E.S.S. Collaboration, et al. 2017, A&A, 600, A89
Hewitt, A., & Burbidge, G. 1980, ApJS, 43, 57
Kirk, J. G., & Mastichiadis, A. 1989, A&A, 213, 75
Kovalev, Yu. A., Kardashev, N. S., Kovalev, Y. Y., et al. 2020, Advances in Space Research, 65, 745
Mastichiadis, A., & Kirk, J. G. 1995, A&A, 295, 613
Mastichiadis, A., Protheroe, R. J., & Kirk, J. G. 2005, A&A, 433, 765
Mastichiadis, A., Petropoulou, M., & Dimitrakoudis, S. 2013, MNRAS, 434, 2684
McLure, R. J., & Dunlop, J. S. 2002, MNRAS, 331, 795
Petropoulou, M., & Mastichiadis, A. 2011, A&A, 532, A11
Petropoulou, M. 2014, A&A, 571, A83
Petropoulou, M., & Mastichiadis, A. 2015, MNRAS, 447, 36
Rieger, F. M., & Volpe, F. 2010, A&A, 520, A23
Shimmins, A. J., & Bolton, J. G. 1974, Aust. J. Phys. Astrophys. Suppl., 32, 1
Sikora M., Kirk J. G., Begelman M. C., & Schneider P. 1987, ApJ, 320, L81
Vestrand, W. T., Stacy, J. G., & Sreekumar, P. 1995, ApJ, 454, L93
Waxman E., & Bahcall J. 1997, Phys. Rev. Lett., 78, 2292
Weidinger, M., & Spanier, F. 2015, A&A, 573,7
Yan, D. H., & Zhang, L. 2015, MNRAS, 447, 2810
Zech, A., Cerruti, M., & Mazin, D. 2017, A&A, 602, 25
Zheng, Y. G., Yang, C. Y., & Kang, S. J. 2016, A&A, 585, 8
Franceschini, A., Rodighiero, G., & Vaccari, M. 2008, A&A, 487, 83